Superlattices and Microstructures 75 (2014) 72–78

Contents lists available at ScienceDirect

Superlattices and Microstructures

journal homepage: www.elsevier.com/locate/superlattices

Rectifying characteristics of a Fe:$SrTiO_3$/Nb:$SrTiO_3$ homojunction

Xiangbiao Qiu, Xiaoyu Zhou, Aidong Li, Zhengbin Gu *, Di Wu *

National Laboratory of Solid State Microstructures, Nanjing University, Nanjing 210093, China
Department of Materials Science and Engineering, College of Engineering and Applied Sciences, Nanjing University, Nanjing 210093, China

ARTICLE INFO

Article history:
Received 31 May 2014
Received in revised form 10 July 2014
Accepted 15 July 2014
Available online 28 July 2014

Keywords:
Laser deposition
Epitaxial growth
Perovskite
$SrTiO_3$

ABSTRACT

Fe-doped $SrTiO_3$ (Fe:STO) thin films have been deposited epitaxially on Nb-doped $SrTiO_3$ (Nb:STO) substrates to form a homojunction. Rectifying characteristics of the Fe:STO/Nb:STO homojunction are studied as a function of temperature. The current under reverse bias is observed to increase dramatically with decreasing temperature. This increased reverse current is ascribed to direct tunneling from the valence band of Fe:STO into the conduction band of Nb:STO, by taking into account the temperature and bias dependence of the dielectric constant of $SrTiO_3$.

1. Introduction

Oxide-electronics is an emerging area that has attracted great attention from both academia and electronic industry, owning to the broad spectrum of electronic properties that functional oxides have from superconductivity, metallic conduction, semiconductivity to insulation [1–3]. High carrier densities and short electronic length scales in oxides are desirable for device miniaturization [3]. Moreover, complex oxides also show ferroelectric, ferromagnetic, multiferroic, opto-electronic, piezoelectric and thermoelectric functionalities that provide agile coupling between different physical entities [3,4]. Oxide-electronics may be a valuable extension and addition to currently ubiquitous

* Corresponding authors at: Department of Materials Science and Engineering, College of Engineering and Applied Sciences, Nanjing University, Nanjing 210093, China.
E-mail addresses: zbgu@nju.edu.cn (Z. Gu), diwu@nju.edu.cn (D. Wu).

http://dx.doi.org/10.1016/j.spmi.2014.07.024
0749-6036/

semiconductor electronics and has shown great potential in novel information storage and processing devices for future generations [5].

In oxide-electronics, perovskite $SrTiO_3$ (STO) may play an important role. Due to limited lattice mismatch, STO is a suitable substrate material for deposition of a number of important functional perovskites ranging from superconducting cuprates, ferroelectric titanates to colossal magnetoresistive manganites. Moreover, high-quality STO thin films can be grown epitaxially on silicon, thereby making STO an appropriate platform to integrate functional oxides and oxide electronic devices with silicon devices [6,7]. *n*-Type doping in STO can be achieved in Nb-doped STO (Nb:STO) by substituting Nb^{5+} for Ti^{4+}, or in La-doped STO by substituting La^{3+} for Sr^{2+} [8–10]. On the other hand, *p*-type STO can be obtained by replacing Ti^{4+} with lower valence cations [11–14]. However, there are also arguments that *p*-type doping may be easily compensated in STO [15].

Junctions where different materials meet at the interface, form the most elementary devices in electronic circuits. Investigations on transport characteristics of oxide junctions are indispensable to make functional oxide electronic devices [16]. In this paper, we report temperature dependent transport characteristics of Fe:STO/Nb:STO homojunctions. It is observed that tunneling current becomes significant with decreasing temperature. This is discussed in terms of the decrease of junction width with decreasing temperature due to the unique temperature and bias dependence of the dielectric constant (ϵ_r) of STO.

2. Experimental

Epitaxial Fe:STO thin films were deposited on (001) Nb:STO (0.5 wt% Nb) substrates, 500 μm in thickness, by pulsed laser deposition (AdNaNo Corp.) from a single-crystalline Fe:STO (0.5 wt% Fe) target, using a Coherent CompexPro 205F KrF excimer laser with a 248 nm output at 4 Hz repetition. The energy density on target was estimated as ~1.5 J/cm^2. The deposition was performed under an oxygen pressure around 0.5 Pa and at a substrate temperature of 800 °C. X-ray diffraction (XRD) of the Fe:STO/Nb:STO junctions was performed at the BL14B1 beam line in Shanghai Synchrotron Radiation Facility. The X-ray wavelength used is 1.2378 Å. Surface morphology of the Fe:STO films was characterized using an Asylum Research Cypher atomic force microscope (AFM). Temperature-dependent transport measurements were performed using a Keithley 2636 source-measure unit on a LakeShore CRX-4K probe station. The voltage was applied on Fe:STO with Nb:STO grounded through indium contact pads.

3. Results and discussions

Fig. 1(a) shows the XRD pattern of an Fe:STO thin films deposited on Nb:STO substrates around the (002) diffraction peak of Nb:STO. A strong diffraction peak from the (002) crystalline plane of the Fe:STO/Nb:STO heterostructure is observed with clear thickness fringes. Diffractions from Fe:STO cannot be distinguished from those from the Nb:STO substrate due to identical lattice constants. The slow damping of the intensity in thickness fringes demonstrates both a smooth film surface and a sharp interface. The film thickness, estimated from the period of the thickness fringes, is ~147 nm. Fig. 1(b) shows the surface AFM image of the Fe:STO film. Atomic steps with a height of ~0.4 nm, close to the height of a unit cell, can be observed. The root-mean-square roughness is estimated about 0.15 nm over a 3 μm × 3 μm area.

The transport characteristics of the Fe:STO/Nb:STO homojunction are shown in Fig. 2, as a function of temperature. At room temperature, a clear rectifying character is observed. The current increases with increasing forward bias rapidly, but keeps negligible with increasing reverse bias applied to Fe:STO up to −2.0 V. However, this rectifying character weakens with decreasing temperature as the reverse current increases dramatically. The inset shows In(I) versus eV/kT at various temperatures, which exhibits a linear relation at low forward voltages, in agreement with the empirical transport relation $I = I_s \exp(eV/\eta kT)$, where I_s is the saturation current under reverse bias and η the ideality factor [17]. At room temperature, $\eta \approx 2.2$, indicative of a recombination-dominated current. The recombination process, with $\eta = 2$, is well described by the Shockley–Read–Hall model [19], where electrons and holes are captured by a single defect level. However, η of the Fe:STO/Nb:STO junction increases

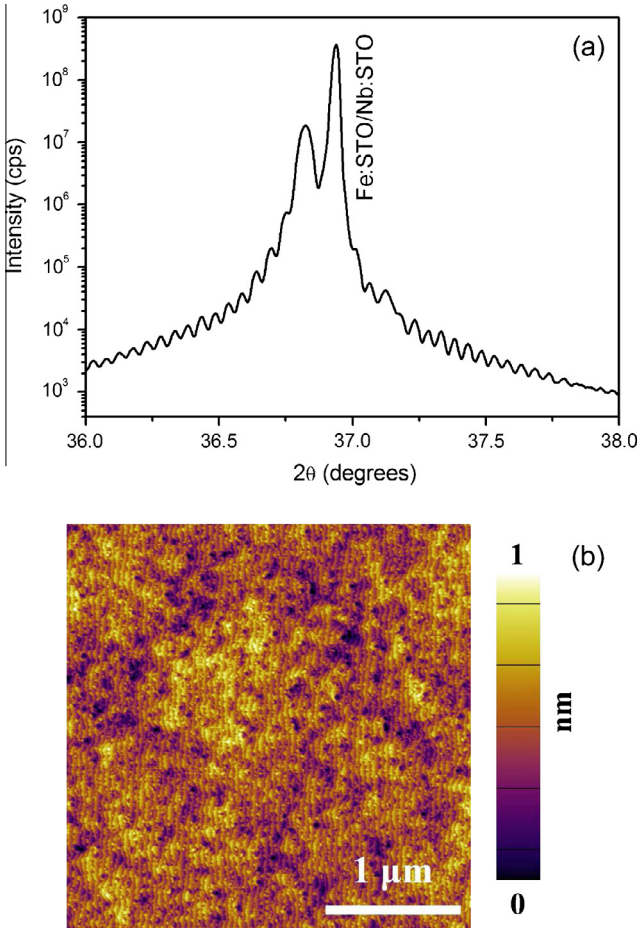

Fig. 1. (a) XRD pattern and (b) surface morphology of a Fe:STO thin film deposited on (001) Nb:STO substrate.

with decreasing temperature to about 3.6 at 200 K and about 7.0 at 120 K. Although an η value greater than 2 is often observed in p–n junctions [20,21], it cannot be explained by the Shockley–Read–Hall model. Instead, the high ideality factor may be ascribed to trap-assisted tunneling [22].

There are evidences that Fe-doping in STO behaves as acceptors [14,23], although only a part of Fe^{3+} ions substitute Ti^{4+} ions in the perovskite lattice [23]. The fermi level of Fe:STO gets closer to the valance band maximum as Fe concentration increases [24]. To explain the transport characteristics observed, we consider a p–n junction as shown in the inset of Fig. 3(a), taking into account the temperature and bias dependence of the dielectric constant of STO based on the analyses provided by Susaki and colleagues [18]. The dielectric constant of Fe:STO and Nb:STO is assumed to follow the same dependence. According to Susaki et al. [18]

$$\epsilon_r(E) = b \Big/ \sqrt{a + E^2}, \tag{1}$$

where $a(T) = [b(T)/\epsilon_r(T, E = 0)]^2$, $b(T) = 1.37 \times 10^9 + 4.29 \times 10^7 T$ V/m and E is the electric field. $\epsilon_r(T, E = 0)$ follows Barrett's formula [25],

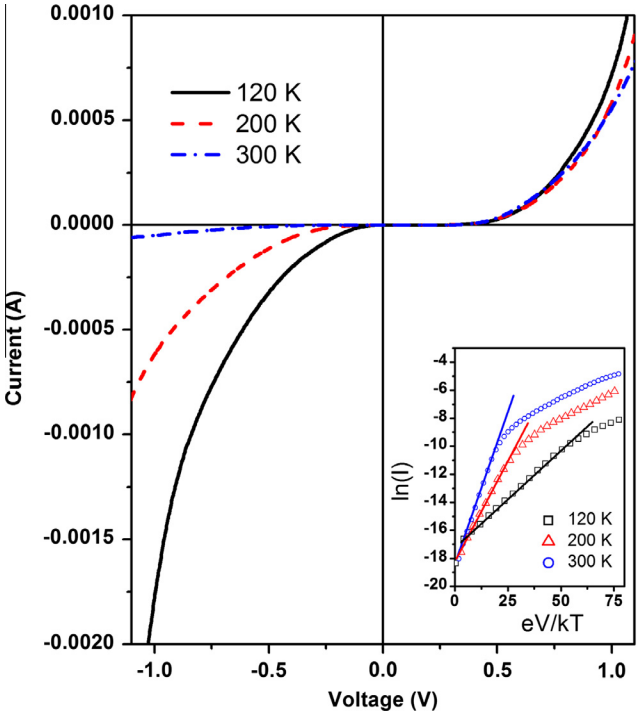

Fig. 2. *I–V* curves of the Fe:STO/Nb:STO *p–n* junction at various temperatures.

$$\epsilon_r(T, E=0) = 1635 \Big/ \left[\coth\left(\frac{44.1}{T}\right) - 0.937\right]. \tag{2}$$

Taking $\epsilon_r(E)$ into the Poisson equation, the electrostatic potential in the junction can be solved as,

$$\psi(x) = \begin{cases} \phi_{bi} - \frac{\sqrt{a}\epsilon_0 b}{eN_D}\left[\cosh\frac{eN_D(x+w_D)}{\epsilon_0 b} - 1\right] & -w_D < x \le 0 \\ \frac{\sqrt{a}\epsilon_0 b}{eN_A}\left[\cosh\frac{eN_A(x-w_A)}{\epsilon_0 b} - 1\right] & 0 < x < w_A, \end{cases} \tag{3}$$

where N_A and N_D are doping concentrations in Fe:STO and Nb:STO, respectively, w_A and w_D the depletion width in Fe:STO and Nb:STO, respectively, e the electron charge, ϵ_0 the dielectric constant of vacuum, and $\phi_{bi} = \psi(-w_D) - \psi(w_A)$ is the build-in potential in the junction in equilibrium.

The carrier concentration in Nb:STO is reported from 10^{19} to 10^{21} cm^{-3} according to different Nb compositions and donor activation treatments [8,26,27]. A medium value $N_D = 10^{20}$ cm^{-3} is adopted in this work. There is little information in the literature on the carrier concentration in Fe:STO. However, due to the compensation in *p*-type STO [15], it is reasonable that N_A is much smaller than that in the Nb:STO substrate. We assume it to be 2.0×10^{19} cm^{-3}. The fermi level of a lightly doped Nb:STO is reported 40 meV above the conduction band minimum [28]. First-principles calculations found that the Fe^{3+} defect level is 1.1 eV above the valence band maximum [29]. The band gap of STO is about 3.2 eV [28]. Therefore, the build-in barrier height in the *p–n* junction $-e\phi_{bi}$ is taken to be -2.0 eV for the calculations. Fig. 3 shows the junction energy barrier at various temperature and bias. Since N_D is much larger than N_A, the depleted space charge region falls almost completely in Fe:STO, the *p*-type region. It is clear that the depletion width decreases dramatically with decreasing temperature. At a certain temperature, 130 K as shown for example in Fig. 3(b), a forward bias increases the depletion width while a reverse bias decreases it.

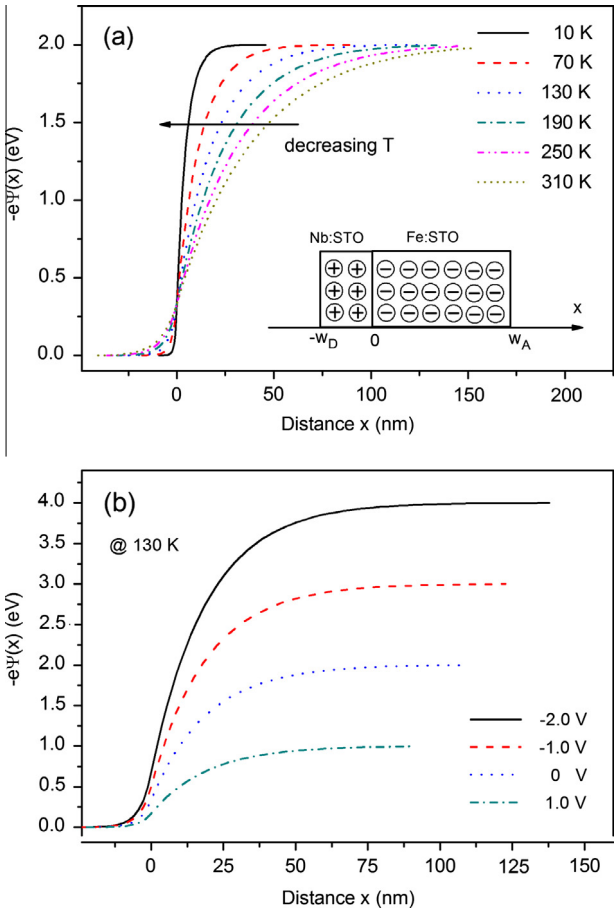

Fig. 3. Calculated energy barrier in the Fe:STO/Nb:STO p–n junction at various temperature (a) and bias (b). The inset in (a) shows a sketch of the junction used for the calculations. The origin of the coordination is set at the junction interface.

The low temperature characteristics, distinctly different from that of conventional semiconductors, stem from the unique temperature and bias dependence of ϵ_r in STO. Susaki et al. [18] reported an increase of tunneling current contribution with decreasing temperature in a Au/Nb:STO Schottky junction, where the barrier width is significantly reduced at low temperatures due to the decrease of ϵ_r in STO near the interface. The simulation results shown in Fig. 3 are in agreement with the previous report. Based on these, band diagrams in this STO p–n junction are proposed as shown schematically in Fig. 4. The key feature, in line with the above simulations, is the decrease in width of the depletion region at low temperatures. Under forward bias, diffusion and recombination currents are suppressed at low temperatures. But the decreased depletion width makes it easier for electrons to recombine through tunneling into defect levels in the band gap of Fe:STO. This results in an increase of η with decreasing temperature, as observed in Fig. 2. Under reverse bias, the decreased depletion width may facilitate direct tunneling from the valence band of Fe:STO into the conduction band of Nb:STO, similar to that in a backward diode [30].

4. Summary

In summary, we fabricated STO homojunctions by depositing Fe:STO thin films on top of Nb:STO substrates. Rectifying characteristics are observed at room temperature. With decreasing temperature,

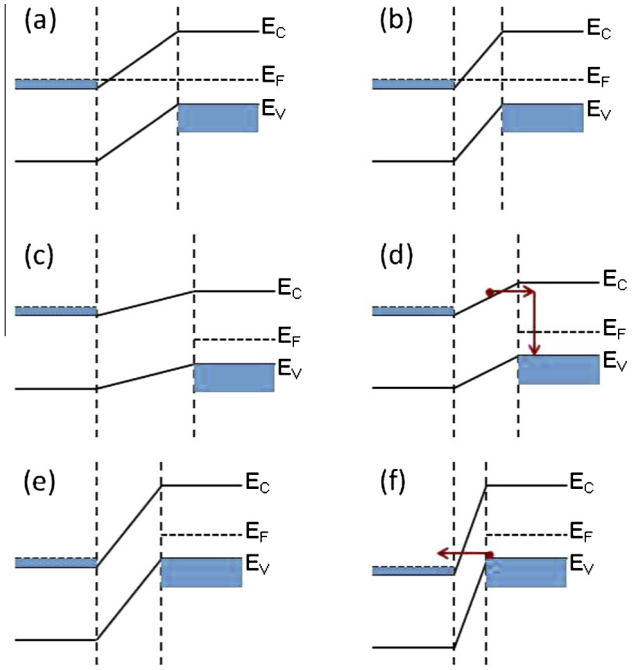

Fig. 4. Schematic band diagrams of the Fe:STO/Nb:STO *p–n* junction at high temperature (a, c, e) and low temperature (b, d, f) in equilibrium (a, b), forward bias (c, d) and reverse bias (e, f). For clarity, the depletion region, between the two vertical dotted lines, is drawn completely in *p*-type Fe:STO.

the reverse current increases dramatically. This peculiar transport behavior are explained in terms of decreases depletion width with decreasing temperature. The decreased depletion width, which stems from the unique temperature and bias dependence of the dielectric constant of STO, increases the tunneling contribution under both forward and reverse bias.

Acknowledgements

This work was jointly sponsored by Natural Science Foundation of China (51222206 and 11374139), Natural Science Foundation of Jiangsu Province (BK2012016) and PAPD project of Jiangsu Province. Shanghai Synchrotron Radiation Facility is greatly acknowledged for providing the beam time and technical assistance.

References

[1] S.D. Ha, S. Ramanathan, J. Appl. Phys. 110 (2011) 071101.
[2] H. Akinaga, Jpn. J. Appl. Phys. 52 (2012) 100001.
[3] D.G. Schlom, L.-Q. Chen, X.Q. Pan, A. Schmehl, M.A. Zurbuchen, J. Am. Ceram. Soc. 91 (2008) 2429.
[4] P. Zubko, S. Gariglio, M. Gabay, P. Ghosez, J.-M. Triscone, Annu. Rev. Condens. Matter Phys. 2 (2011) 141.
[5] Y. Tokura, H.Y. Hwang, Nat. Mater. 7 (2008) 694.
[6] M.P. Warusawithana, C. Cen, C.R. Sleasman, J.C. Woicik, Y. Li, L.F. Kourkoutis, J.A. Klug, H. Li, P. Ryan, L.P. Wang, M. Bedzyk, D.A. Muller, L.Q. Chen, J. Levy, D.G. Schlom, Science 324 (2009) 367.
[7] J.W. Reiner, A.M. Kolpak, Y. Segal, K.F. Garrity, S. Ismail-Beigi, C.H. Ahn, F.J. Walker, Adv. Mater. 22 (2010) 2919.
[8] J.F. Schooley, W.R. Hosler, M.L. Cohen, Phys. Rev. Lett. 12 (1964) 474.
[9] A. Leitner, D. Olaya, C.T. Rogers, J.C. Price, Phys. Rev. B 62 (2000) 1408.
[10] D. Olaya, F. Pan, C.T. Rogers, J.C. Price, Appl. Phys. Lett. 84 (2004) 4020.
[11] R. Waser, J. Am. Ceram. Soc. 74 (1991) 1934.
[12] T. Higuchi, T. Tsukamoto, N. Sata, M. Ishigame, Y. Tezuka, S. Shin, Phys. Rev. B 57 (1998) 6978.
[13] Y.S. Dai, H.B. Lu, F. Chen, Z. H Chen, Z.Y. Ren, D.H.L. Ng, Appl. Phys. Lett. 80 (2002) 3545.

[14] I. Denk, W. Munch, J. Maier, J. Am. Ceram. Soc. 78 (1995) 3265.
[15] J. Robertson, S.J. Clark, Phys. Rev. B 83 (2011) 075205.
[16] T. Yajima, Y. Hikita, H.Y. Hwang, Nat. Mater. 10 (2011) 198.
[17] S.M. Sze, K.K. Ng, Physics of Semiconductor Devices, third ed., John Wiley & Sons, New Jersey, 2007. pp. 79.
[18] T. Susaki, Y. Kozuka, Y. Tateyama, H.Y. Hwang, Phys. Rev. B 76 (2007) 155110.
[19] W. Shockley, W.T. Read, Phys. Rev. 87 (1952) 835.
[20] L. Esaki, Phys. Rev. 109 (1958) 603.
[21] J.M. Shah, Y.-L. Li, Th. Gessmann, E.F. Schubert, J. Appl. Phys. 94 (2003) 2627.
[22] A.G. Chynoweth, W.L. Feldmann, R.A. Logan, Phys. Rev. 121 (1961) 684.
[23] J. Szadea, K. Szotab, M. Kulpaa, J. Kubackia, Ch. Lenserb, R. Dittmann, R. Waser, Phase Trans. 84 (2011) 489.
[24] C. Lenser, Dissertation at RWTH Aachen University, 2013.
[25] J.H. Barrett, Phys. Rev. 86 (1952) 118.
[26] E.R. Pfeiffer, J.F. Schooley, Phys. Lett. 29A (1969) 589.
[27] C.S. Koonce, M.L. Cohen, J.F. Schooley, W.R. Hosler, E.R. Pfeiffer, Phys. Rev. 163 (1967) 380.
[28] M. Takizawa, K. Maekawa, H. Wadati, T. Yoshida, A. Fujimori, H. Kumigashira, M. Oshima, Phys. Rev. B 79 (2009) 113103.
[29] X. Zhou, J. Shi, C. Li, J. Phys. Chem. C 115 (2011) 8305.
[30] J.B. Hopkins, Solid-State Electron. 13 (1970) 697.